

11th ANKARA INTERNATIONAL AEROSPACE CONFERENCE
8-10 September 2021 - METU, Ankara TURKEY

AIAC-2021-017

STAR SIMULATOR DESIGN FOR STAR TRACKER DEVELOPMENT

Nevsan Sengil¹
University of Turkish Aeronautical Association
Ankara, Turkiye

Omar B. Stambouli²
Saad Dahleb University
Blida, Algeria

ABSTRACT

Different sensors such as horizon sensors, sun sensors, magnetic field sensors and star trackers are deployed to determine attitude of the spacecrafts. Star tracker is the most sensitive sensor among those to determine spacecraft's orientation in an inertial frame. We can use a variety of test settings to develop star trackers. In one case, both star tracker and stars simulated using software. In the next case, a physical star tracker and simulated stars on a computer screen are used. Finally, as a last alternative we can test star trackers with real stars on the sky. In this study, we developed an artificial digital camera which generates star images from star catalogs. Although stars are point sources, their light are spread on the digital images imitating Gaussian function called point spread function. Consequently, a relation between star visual magnitude and standard deviation of point spread function is developed using regression analysis. As a result, artificial star images converge real ones. As a next step, we compared both real images taken by satellite and artificial images generated by our software. Both, software produced, and real images are visually found very similar.

INTRODUCTION

Space race was started when humans heard the first telemetry signal of the Sputnik in 1957. Thousands of spacecrafts were designed, produced, and launched to date. A high percentage of spacecrafts launched from Earth are orbited in LEO (Low Earth Orbit). Comparatively small number of spacecrafts are either in MEO (Medium Earth Orbit) or GEO (Geosynchronous Orbit). In the meantime, a smaller number of spacecrafts were assigned to travel in our solar systems in either in Sun or in solar system's frontier's direction. Five of these spacecrafts named Voyager-1, Voyager-2, Pioneer-1, Pioneer-2, and New Horizons were aimed to leave our solar system and continue their journey into the interstellar. For collecting data and communicating with Earth, not only navigation of these spacecrafts on the correct orbits but also the directions of them are utmost important. Although magnetic field sensors, sun sensors, horizon sensors and Earth sensors are available to determine the orientation of the spacecraft, star trackers are the most sensitive sensor among these [Wang et al., 2019].

Performance tests of the star trackers on the ground is very crucial. Because, once spacecraft is launched, there is no way to repair the star tracker units. The most natural way to test star

¹ Prof. in Astronautical Engineering Department, Email: nsengil@thk.edu.tr

² Master Student in Institute of Aeronautics and Space Studies, Email: omar.boudghene@spacegeneration.org

trackers is to use real stars in the sky. However, using the real stars require nighttime, good weather conditions, and geographic territories unpolluted with light [Ardi et al., 2018]. The second alternative is to use star simulators. These star simulators are either software-only or software-hardware hybrid systems. In software-only systems, digital star images are directly fed into star tracker's image segmentation unit by-passing optical units and digital camera. Here additional tests are required for these units. In software-hardware hybrid systems however, star simulator projects stars on a display and star tracker's digital camera unit are directed to these artificial stars. The advantage is both optical systems and digital camera are included in these tests. Both type of star simulators can shorten development time and cut down test expenses.

In this study, we propose a software-only star tracker test bed. Our proposed test setting is both faster and more economical than field tests and software-hardware hybrid systems. However, star tracker's optical units are not included in these tests and may require additional tests.

STAR SIMULATIONS

Star Catalogs

Star trackers use star catalogs to identify the stars. Once two stars are identified, orientation of the spacecraft can be estimated with various algorithms such as Triad or Quest.

It is estimated that there are more than 400 billion stars only in our Milky Way galaxy. To search, find and observe so many stars is a non-trivial task. Consequently, only a limited number of stars are listed in star catalogs. Star catalogs contain some additional details about listed stars.

These details are classified in two sub-group as astrometric or photometric [Schulz, 2021]. Astrometric data consist of star positions given by celestial coordinates, their rate of change called as annual proper motions, and trigonometric parallaxes.

Photometric data consist of visual magnitudes of the stars in different bands of the electromagnetic radiation such as B (blue), V (visual), I (infrared), and U (ultraviolet).

The most common star catalogs are BSC (Yale Bright Star Catalog), SAO (Smithsonian Astrophysical Observatory), USNO-B1.0 (U.S. Naval Observatory), GSC (Guide Star Catalog), Tycho and Hipparcos (Table-1).

Catalog	HIP	BSC	SAO	USNO-B1.0	GSC	TYCHO
No of stars	118.218	9100	258.996	~1 B	~19 M	~1 M
Max V	12.5	6.5	9	21	15	11.5

Hipparcos Star Catalog

In this study we used Hipparcos Star Catalog constructed by ESA (European Space Agency). There are around 118000 stars in this star catalog (Figure 1). Mostly, the stars with visual magnitude brighter than 12.5 are included (<https://www.cosmos.esa.int>). Epoch date for the Hipparcos star catalog is J1991.25.

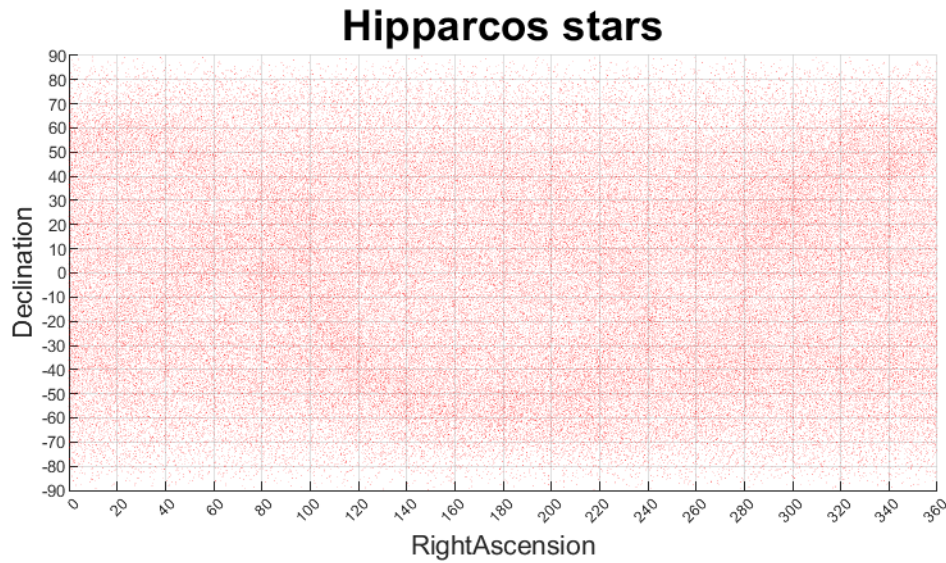


Figure 1: J1991.25-star positions in Hipparcos star catalog

Hipparcos catalog gives the details of the stars such as HIP number, RA (Right Ascension), Dec (Declination), V (magnitude), π (parallax), and μ_α, μ_δ (proper motion) values as in Figure 2.

Number HIP	Descriptor: epoch J1991.25						Position: epoch J1991.25				Par. π mas	Proper Motion	
	RA h m s	Dec \pm° ' "	V mag				α (ICRS) deg	δ deg		μ_α mas/yr		μ_δ	
1 2	3	4	5	6	7	8	9	10	11	12	13		
1	00 00 00.22	+01 05 20.4	9.10	H		0.000 911 85	+01.089 013 32		3.54	-5.20	-1.88		
2	00 00 00.91	-19 29 55.8	9.27	G		0.003 797 37	-19.498 837 45	+	21.90	181.21	-0.93		
3	00 00 01.20	+38 51 33.4	6.61	G		0.005 007 95	+38.859 286 08		2.81	5.24	-2.91		
4	00 00 02.01	-51 53 36.8	8.06	H		0.008 381 70	-51.893 546 12		7.75	62.85	0.16		
5	00 00 02.39	-40 35 28.4	8.55	H		0.009 965 34	-40.591 224 40		2.87	2.53	9.07		
6	00 00 04.35	+03 56 47.4	12.31	G		0.018 141 44	+03.946 488 93		18.80	226.29	-12.84		
7	00 00 05.41	+20 02 11.8	9.64	G		0.022 548 91	+20.036 602 16		17.74	-208.12	-200.79		
8	00 00 06.55	+25 53 11.3	9.05	3 H		0.027 291 60	+25.886 474 45		5.17	19.09	-5.66		
9	00 00 08.48	+36 35 09.4	8.59	H		0.035 341 89	+36.585 937 77		4.81	-6.30	8.42		
10	00 00 08.70	-50 52 01.5	8.59	H		0.036 253 09	-50.867 073 60		10.76	42.23	40.02		
11	00 00 08.95	+46 56 24.0	7.34	H		0.037 296 95	+46.940 001 54		4.29	11.09	-2.02		
12	00 00 09.82	-35 57 36.8	8.43	H		0.040 917 56	-35.960 224 82		4.06	-5.99	-0.10		
13	00 00 10.00	-22 35 40.9	8.80	H		0.041 679 70	-22.594 680 60		3.49	8.45	-10.07		
14	00 00 11.59	-00 21 37.5	7.25	G		0.048 271 89	-00.360 421 19		5.11	61.75	-11.67		
15	00 00 12.07	+50 47 28.2	8.60	H		0.050 308 90	+50.791 173 84		2.45	13.88	5.47		
*16	00 00 12.34	-54 54 50.9	11.71	G		0.051 408 52	-54.914 128 19		0.53	257.39	-96.63		
*17	00 00 12.26	-40 11 32.4	8.15	H		0.051 099 57	-40.192 328 42		6.15	-34.46	-26.37		
18	00 00 12.75	-04 03 13.5	11.03	G		0.053 139 23	-04.053 738 13		19.93	-127.22	23.78		
19	00 00 12.80	+38 18 14.7	6.53	H		0.053 316 96	+38.304 086 36		4.12	-2.50	-15.07		
20	00 00 15.11	+23 31 45.4	8.51	G		0.062 950 50	+23.529 283 97		10.76	36.00	-22.98		
21	00 00 15.90	+08 00 26.0	7.55	H		0.066 235 69	+08.007 234 37		5.84	61.89	-0.22		
22	00 00 16.83	-49 21 08.2	8.69	H		0.070 135 93	-49.352 266 86		4.47	-7.90	0.46		
23	00 00 17.86	+13 18 44.0	7.57	G		0.074 429 30	+13.312 210 83		12.21	54.15	9.65		
24	00 00 18.25	-23 27 09.9	9.05	H		0.076 049 79	-23.452 749 13		9.73	127.15	22.22		
25 H	00 00 19.05	-44 17 25.1	6.28	G		0.079 365 37	-44.290 297 41	A	13.74	58.36	-108.64		

Figure 2: Hipparcos astrometric data used by star trackers

Star coordinates and proper motions are defined with ICRS (International Celestial Reference System) in Hipparcos star catalog [Camargo, Teixeira, and Benevides-Soares, and Ducourant, 2001]. ICRS is consisted with the equatorial coordinates (Figure 3).

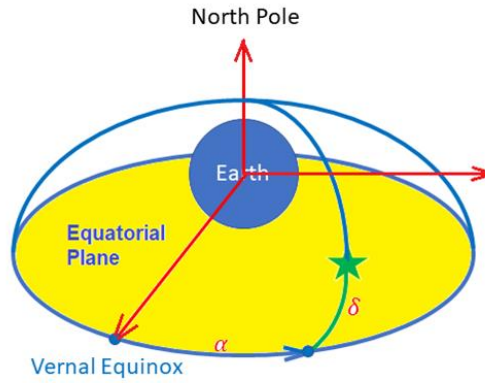


Figure 3: Equatorial coordinate system

Photometric data consist of in different color bands such as B-V (blue-445 nm, V (visual-551 nm) and V-I (infrared-806 nm) in the Johnson BVV system (Figure 4).

No. HIP	Tycho Magnitudes					Colour Indices						Magnitude (Hp)					Variability (Hp)			
	B _r mag	σ mag	V _r mag	σ mag		B-V mag	σ mag		V-I mag	σ mag		Hp mag	σ mag	s mag	N	Max mag	Min mag	P days		
31	32	33	34	35	36	37	38	39	40	41	42-3	44	45	46	47	48	49	50	51	52-4
1	9.643	0.020	9.130	0.019		0.482	0.025	T	0.55	0.03	L	9.2043	0.0020	0.017	87	9.17	9.24			
2	10.519	0.033	9.378	0.021		0.999	0.002	G	1.04	0.00	I	9.4017	0.0017	0.015	120	9.37	9.44		C	
3	6.576	0.004	6.621	0.005		-0.019	0.004	G	0.00	0.00	H	6.6081	0.0007	0.008	127	6.60	6.62		C	
4	8.471	0.007	8.092	0.007		0.370	0.009	T	0.43	0.01	L	8.1498	0.0011	0.015	201	8.12	8.18			
5	9.693	0.014	8.656	0.010		0.902	0.013	T	0.90	0.01	L	8.7077	0.0018	0.019	161	8.68	8.74			
6						1.336	0.020	G	1.55	0.03	I	12.4488	0.0085	0.091	87	12.30	12.60			
7	10.542	0.039	9.679	0.030		0.740	0.020	G	0.79	0.02	H	9.6795	0.0021	0.017	104	9.65	9.72		C	
8	10.433	0.055	9.151	0.029		1.102	0.051	T	3.92	0.39	O	8.5522	0.1671	1.460	77	7.15	11.25	327.50	P 1 B	
9	9.962	0.025	8.711	0.015		1.067	0.023	T	1.03	0.02	L	8.7534	0.0018	0.014	107	8.73	8.78		C	
10	9.140	0.011	8.630	0.010		0.489	0.011	T	0.56	0.01	L	8.6994	0.0020	0.019	156	8.66	8.75			
11	7.446	0.005	7.364	0.005		0.081	0.007	T	0.09	0.01	L	7.3777	0.0010	0.012	153	7.36	7.40		C	
12	10.369	0.023	8.588	0.010		1.484	0.020	T	1.50	0.03	L	8.5598	0.0012	0.017	177	8.53	8.59			
13	10.216	0.026	8.887	0.014		1.128	0.023	T	1.09	0.02	L	8.9707	0.0017	0.015	117	8.94	9.00			
14	8.812	0.013	7.396	0.008		1.200	0.015	G	1.16	0.01	H	7.4195	0.0009	0.009	97	7.41	7.43		C	
15	10.117	0.020	8.739	0.011		1.166	0.018	T	1.13	0.02	L	8.7669	0.0018	0.022	192	8.73	8.80			

Figure 4: Hipparcos photometric data used by star trackers

Star Trackers

Spacecrafts need exact orientation knowledge to direct their antennas, sensors, and thrusters. Currently, star trackers are the most accurate sensors to determine attitude of the spacecrafts. These devices contain very sensitive optical units, digital cameras, processors, software solvers, and look-up tables composed from star catalogs [Toloei, Arayani and Abaszadeh, 2014] (Figure 5).

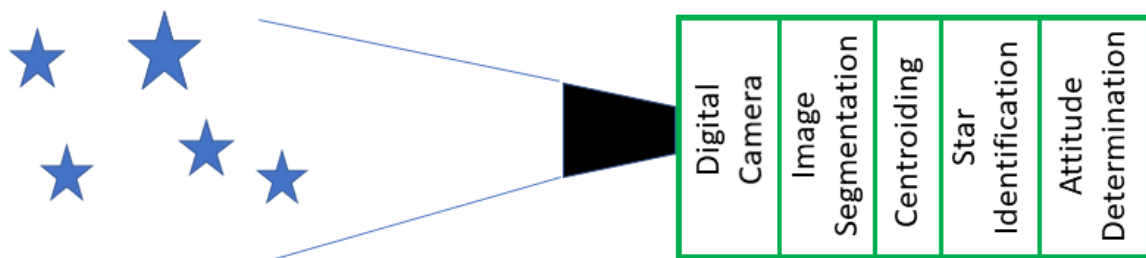


Figure 5: A generic star tracker components

Optical unit collects the light energy coming from stars which positioned in the FOV (field-of-view). This energy is focused on detectors of digital camera. Detectors convert light energy to electronic signals. Next, these electronic signals are stored as raw digital images on the memory unit. Following, raw digital images are processed sequentially by different algorithms on the computer unit. Image segmentation algorithm calculates a threshold value and separates images and background. Then centroiding algorithm calculates exact center of the stars. Finally, star identification algorithm recognizes the stars [Liebe, 1995]. A minimum of two stars are required for attitude determination. To increase computational efficiency, star trackers further cut down both number of stars and details about these stars stored in star tracker's memory. Only the stars brighter than some threshold values are picked up. In addition to star's catalog identification numbers, Dec (declination), RA (right ascension), apparent V (visual magnitude), π (parallax), and μ_α, μ_δ (proper motion) values are kept in star tracker's memory unit.

Point Spread Function (PSF)

Stars are very far away from our solar system. Even the distance to closest star system Alpha Centaury is 4.37 light-years. Consequently, stars are assumed to be point sources. Even if no optical aberration is present, the image of a star is not a point on the digital image. For example, digital image of the Alnilam from Orion constellation is shown in Figure 6. The image's FOV (field-of-view) is $9.6^\circ \times 11.2^\circ$, and pixel numbers are 831×985 in vertical and horizontal directions, respectively. This image is taken from the Asteria CubeSat (<https://www.nasa.gov/feature/jpl/astrophysics-cubesat-demonstrates-big-potential-in-a-small-package>) [Schulz et al., 2021].

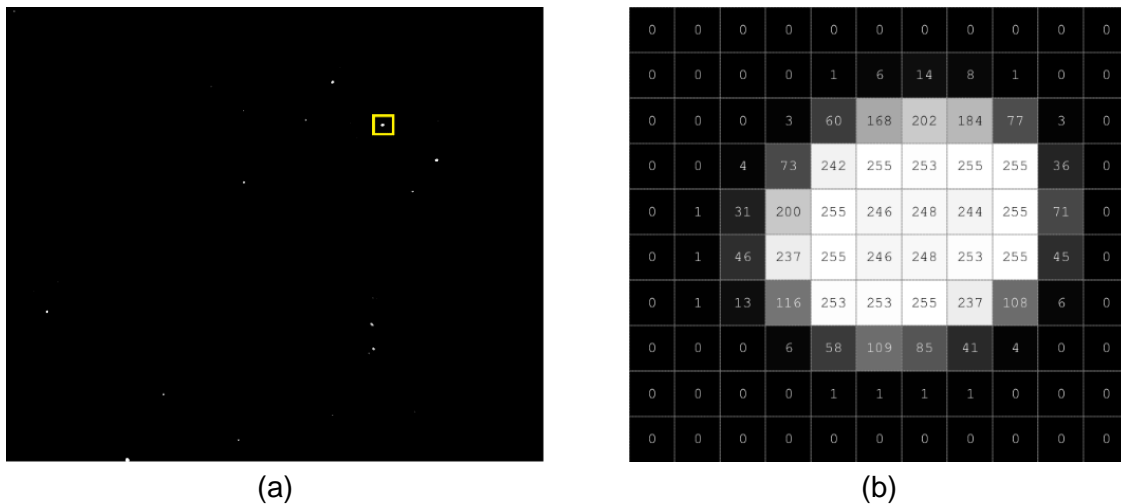


Figure 6: (a) Orion star cluster image taken by Asteria CubeSat (courtesy of NASA) (b) Alnilam's digital image values with 8-bits representation

Two-dimensional form of star light on the focal plane can be described as a PSF (point spread function). Light energy pattern approximately accords with a Gaussian distribution as shown in equation below.

$$f(r, A, \sigma) = A e^{-\frac{r^2}{2\sigma^2}} \quad (1)$$

In this equation, r , A , σ distance from center, constant amplitude, and standard deviation, respectively. The values of PSF for $A = 255$ and different σ values are shown in Figure 7.

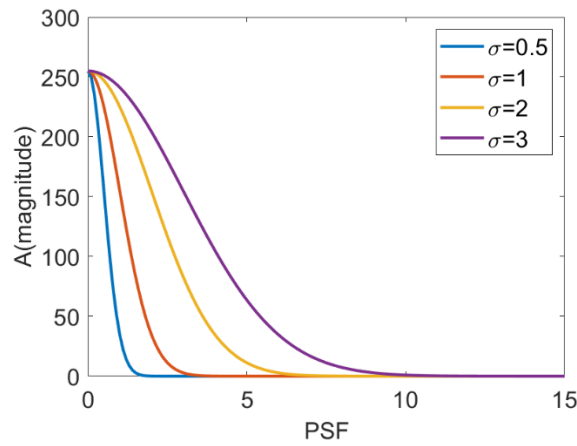


Figure 7: Point spread function for different σ values

ARTIFICIAL STAR IMAGES

In this study, only the stars with visual magnitude lower than 5.2 are considered. In Hipparcos star catalog, there are 2030 stars which visual magnitudes are less than 5.2. FOV of the artificial camera is taken as $10^0 \times 10^0$. Optical axis is directed to Orion star cluster. Some part of the Orion star cluster is located between $76^0 \leq RA \leq 86^0$ and $1.6^0 \leq DEC \leq -8.4^0$. In this region, there are 23 stars with visual magnitudes less than $V < 5.2$ as shown in Figure 8.

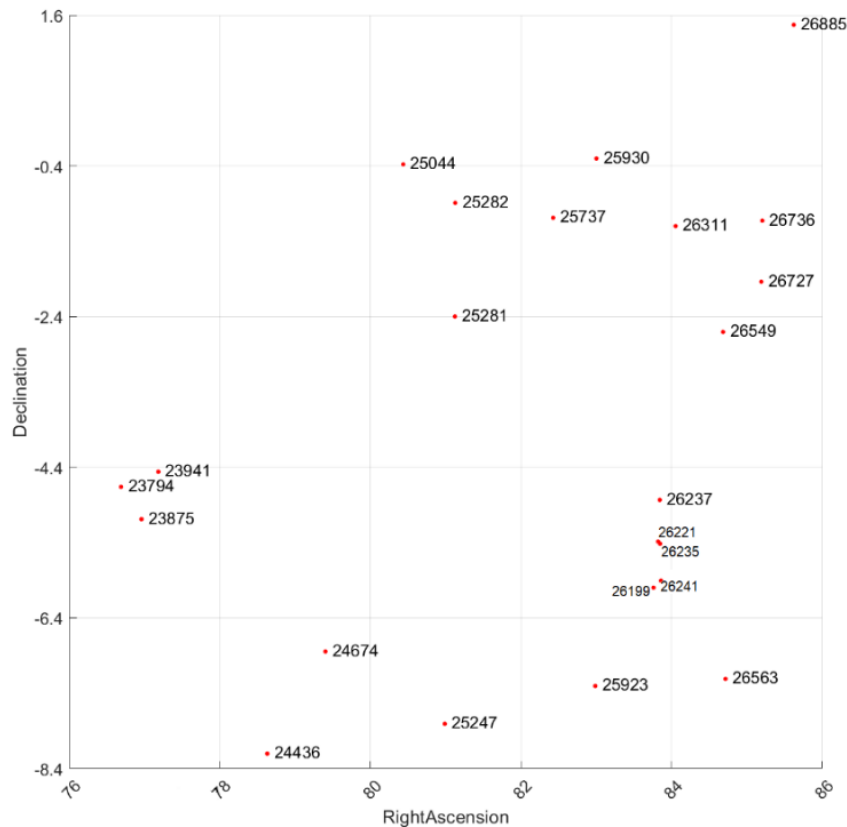


Figure 8: Orion cluster stars with Hipparcos numbers

These stars with their Hipparcos numbers and visual magnitudes are listed in Table-2.

HIP	23941	23794	23875	24674	24436	25044	25282	25281
V	5.11	5.12	2.78	3.59	0.18	4.72	5.07	3.35
HIP	25247	25930	25737	25923	26885	26311	26736	26727
V	4.13	2.25	4.71	4.62	4.9	1.69	4.95	1.74
HIP	26549	26237	26221	26235	26199	26241	26563	
V	3.77	4.58	5.13	4.98	4.78	2.75	4.77	

For statistical purposes, 10 sample stars are chosen, and their photometric characteristics are derived using Orion cluster image from Asteria CubeSat (Figure 6-a) and listed in Table-3.

HIP	24436	26311	26727	25930	23875	24674	25247	25737	26199	23794
V	0.18	1.69	1.74	2.25	2.78	3.59	4.13	4.71	4.78	5.12
Kernel	10 × 10	9 × 9	9 × 9	8 × 8	8 × 8	6 × 6	6 × 6	6 × 6	6 × 6	5 × 5
DN_{max}	255	255	255	255	255	255	244	242	177	41
ΣDN	13108	6782	6344	5228	4095	1987	1669	1449	642	164
E_1/E_2	94.6	23.6	22.5	14.1	8.6	4.1	2.5	1.5	1.4	1

In this Table, HIP, V , kernel, DN_{max} , ΣDN , are star's Hipparcos number, visual magnitude, 2-dimensional PSF pixel size, maximum DN (digital number) in this kernel, total DN's in this kernel. Last term E_1/E_2 is ratio of energy fluxes between two stars which is described by (2) [Markley and Crassidis, 2014]. Visual magnitude of HIP 23794 ($V_2 = 5.12$) is taken as reference for these ratios.

$$\frac{E_1}{E_2} = 10^{-0.4(V_1 - V_2)} \quad (2)$$

Star light is distributed according to PSF function on a kernel. The size of kernel and DNs are functions of both star's visual magnitude, detector sensitivity and pixel size of the digital camera. 2-dimensional PSF is defined by erf (error functions) [Zhang, 2017].

$$I(m, n) = 0.5 D \pi \sigma^2 \left(erf\left(\frac{n}{\sqrt{2}\sigma}\right) - erf\left(\frac{n+1}{\sqrt{2}\sigma}\right) \right) \times \left(erf\left(\frac{m}{\sqrt{2}\sigma}\right) - erf\left(\frac{m+1}{\sqrt{2}\sigma}\right) \right) \quad (3)$$

In this equation, m , n , D , and σ are distance of pixels in x- and y-directions, constant and standard deviation, respectively. In this study, D (constant) is taken as 300 to increase star brightness for easy detection by human eyes. Maximum DN (digital number) we can use on 8-bits image is 255. Then, σ (standard deviation) and V (visual magnitude) values are plotted to better understand their mathematical relationship (Figure 9). Additionally, we applied a regression analysis to predict σ values from star's visual magnitudes.

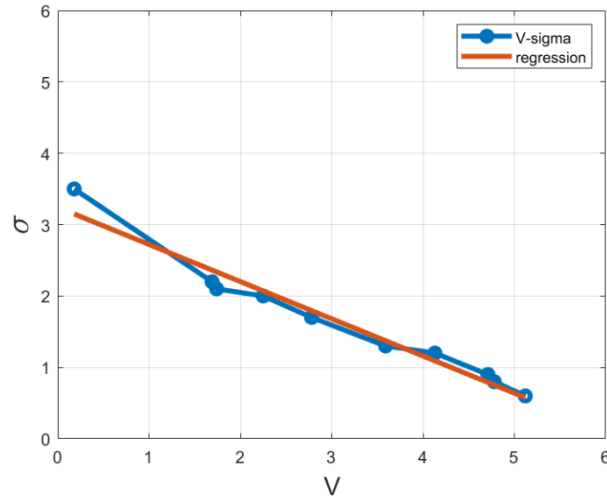


Figure 9: Relations between star visual magnitude and σ

After regression analyses, linear function is calculated as,

$$\sigma = -0.55 \times V + 3.8 \quad (4)$$

Once regression analyses are completed, we calculated a σ for each star given in Table-2 and created artificial stars in Orion cluster using positions taken from Hipparcos star catalog and PSF calculated by σ values. Both images taken from Asteria CubeSat, and artificial image are exhibited in Figure 10. Artificial image consists of 800 pixels in both directions. Although small differences are observed, they are found quite similar.

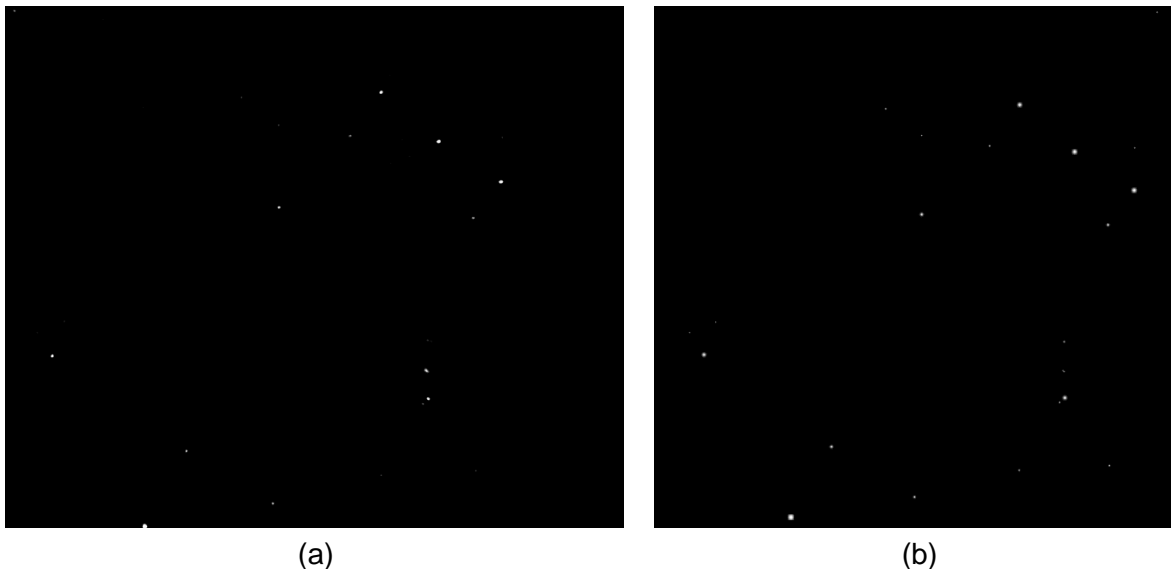
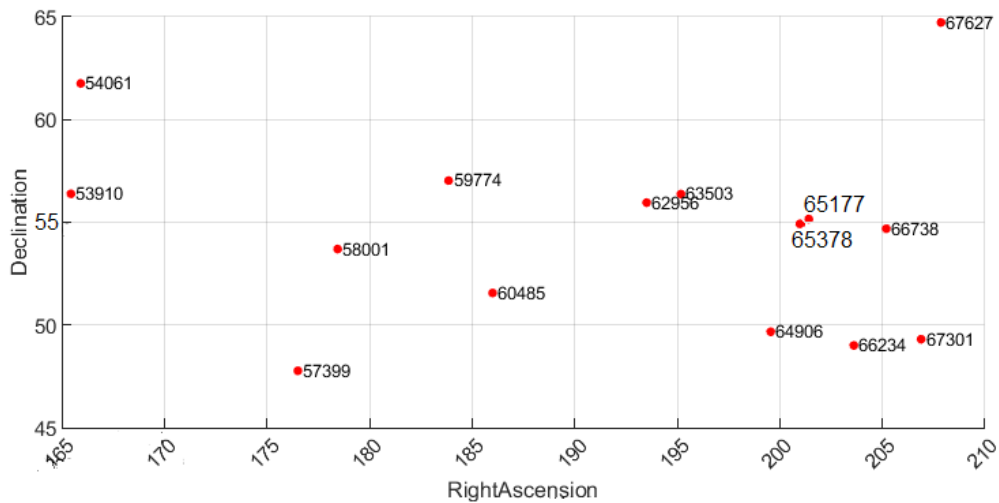


Figure 10: (a) Orion star cluster image taken by Asteria CubeSat (courtesy of NASA) (b) artificial image

As a second case we applied same method to Big Dipper star cluster. This time we changed FOV of our artificial camera to $20^\circ \times 45^\circ$, between $45^\circ \leq DEC \leq 65^\circ$ and $165^\circ \leq RA \leq 210^\circ$ as shown in Figure 11. Image pixel size is 1000×2500 .



(a)



(b)

Figure 11: (a) HIP numbers of stars in Big Dipper cluster (b) Artificial image of stars in Big Dipper

CONCLUSIONS

In this paper, we studied how to artificially create star images as real as possible both in astrometrically and photometrically. A real star image from Orion star cluster is used for comparison purposes. This image is taken with NASA's Asteria CubeSat's digital camera. Simulated stars are copied from Hipparcos star catalog. Only the stars with visual magnitudes lower than 5.2 are picked up. Consequently, we limited number of stars to 2030 in our data base. Next, we developed a photometric function between star's visual magnitude and PSF's standard deviation value using regression analysis. We created artificial digital images of stars, in two different test cases using different FOV angles and pixel numbers. As a next step, we compared real and artificial images based on star visual magnitudes, and positions. Two images are visually matched, yet some small differences are observed. The scope of this study is limited with software-only test system for star trackers. In future studies, we will further develop our test system using high-resolution monitor systems and digital cameras certified for space applications.

References

- Ardi, N.S., Saifudin, M.A., Poetro, R.E., and Fathurrohlim, L., (2018), *Development of star image simulator for star sensor algorithm validation*, 6th International Seminar of Aerospace Science and Technology, IOP Conf. Series, Journal of Physics: Conf. Series 1130 (2018) 012020.
- Camargo, J.I.B., Teixeira, R., Benevides-Soares, P., and Ducourant, C., (2001), *Extension of the ICRF for selected areas down to the 15th magnitude*, Astronomy and Astrophysics, Vol. 375, p: 308-318.
- Liebe, C.C., (1995), *Star trackers for attitude determination*, IEEE Aerospace Electronic Systems Magazine, Vol. 10 (6) p: 10-16.
- Markley F.L. and Crassidis L.C., (2014), *Fundamentals of Spacecraft Attitude Determination and Control*, Springer New York, USA.
- Schulz, V.H. and et al, (2021) *Universal Verification Platform and Star Simulator for Fast Star Tracker Design*, Sensors, Vol. 21, 907.
- Toloei, A.R., Arani, M.S., Abaszade, M., (2014), *A New Composite Algorithm for Identifying the Stars in the Star Tracker*, International Journal of Computer Applications, Vol. 102 (2), p: 28-33.
- Wang, G., Lv, W., Li, J., and Wei, X., (2019), *False Star Filtering for Star Sensor Based on Angular Distance Tracking*, IEEE Access, Vol. 7, p: 62401-62411.
- Zhang, G., (2017), *Star Identification: Methods, Techniques and Algorithms*, Springer: Berlin/Heidelberg, Germany.